coatings

MDPI

Article

Improved Ability to Resist Corrosion of Selective-Laser-Melted Stainless Steel Based on Microstructure and Passivation Film Characteristics

Huimin Tao [1,*], Yafang Cai [2], Zeqi Tong [1], Yong Huang [1] and Mingming Ding [1]

[1] Nanxun Innovation Institute, Zhejiang University of Water Resources and Electric Power, Hangzhou 310018, China
[2] College of Mechanical and Electrical Engineering, China Jiliang University, Hangzhou 310018, China
* Correspondence: taohm@zjweu.edu.cn

Abstract: The local corrosion resistance of forging and selective laser melting (SLM) 304 steels was explored by intergranular corrosion analysis, double-loop electrochemical potentiodynamic reactivation, dynamic polarization experimentation, structural analysis, and passivation film characteristics analysis. The ability to resist sensitization of SLM 304 steel is greater than that of forging 304 steel at a temperature of 650 °C for 9 h. Moreover, the pit corrosion resistance of forging and SLM 304 steels is weakened by sensitization, while the pit corrosion resistance of SLM 304 steel is much greater than that of forging steel. Therefore, SLM technology can improve the ability to resist sensitization and pit corrosion of 304 steel. Analysis showed that the ability to resist corrosion of the passivation film of SLM 304 steel is greater than that of forging steel. In addition, corrosion pits are easier to generate at the interface of forging steel and SLM 304 steel. The grain boundary corrosion of SLM 304 steel intensified while the corrosion of the melt pool boundaries weakened after the sensitization treatment, resulting in a decrease in pit corrosion resistance. The coupling effect of these different structures and passivation films decides the pit and sensitization resistance of forging and SLM 304 steels. Clarifying the corrosion mechanism of forging and SLM steels is of great significance for scientific research and the widespread use of SLM technology.

Keywords: selective laser melting; sensitization; intergranular corrosion; pit corrosion

Citation: Tao, H.; Cai, Y.; Tong, Z.; Huang, Y.; Ding, M. Improved Ability to Resist Corrosion of Selective-Laser-Melted Stainless Steel Based on Microstructure and Passivation Film Characteristics. *Coatings* **2024**, *14*, 589. https://doi.org/10.3390/coatings14050589

Academic Editor: Alicia Esther Ares

Received: 22 April 2024
Revised: 1 May 2024
Accepted: 4 May 2024
Published: 9 May 2024

1. Introduction

Additive manufacturing (AM) technology has become a widely used and important forming technology in various industries in recent years, including in the aviation, automotive, medical, construction, and many other fields [1–3]. The benefits of AM technology compared with previous forming methods are obvious, especially in the production of complex and high-precision components. AM technology can produce a variety of styles of products in a shorter time, significantly improving production efficiency. The impact of AM poses challenges to traditional design and maintenance methods. AM typically uses high-energy lasers or electron beams in a layer-by-layer manner, cyclically increasing and decreasing temperatures over a wide temperature range in a short period time, which is very different from traditional processing techniques. This approach leads to a complicated thermal history, directly affecting the final microstructure and macroscopic properties [4–6]. Therefore, understanding the aforementioned effects of AM special forming technology is necessary to ensure its effective, safe, and long-term use. In AM technology, the selective laser melting (SLM) method is a commonly applied technique in the forming of alloy materials. According to reports [7–9], SLM steel typically has a higher strength, higher tensile ductility, and higher hardness compared to traditional stainless steel. In addition, SLM technology is not only convenient for manufacturing complex metal parts but is also

cost-effective. However, more work is needed to study the microstructure and macroscopic performances of SLM materials to meet their widespread applications.

Stainless steel plays an important role in production and daily life due to its rich variety, stable structure, excellent performance, reasonable price, and environmental friendliness. Therefore, stainless-steel materials are also one of the key alloys of concern in AM alloys. In general, the corrosion properties of metal parts are inevitably considered during their wide application, especially in terms of local corrosion. Among these corrosion behaviors, sensitization and pit corrosion behaviors have always been a hot issue of stainless steel and are an inevitable problem in the application of stainless steel. Traditional forging stainless steel will be damaged by sensitization and pit corrosion in certain environments, which will deteriorate its performance. At present, sensitization and pit corrosion have also attracted wide attention in the additive manufacturing of stainless steel. Macatangay et al. [10] found that the melt pool boundaries (MPBs) in SLM 316L steel were difficult to corrode and accelerated ring breaking, and heat treatment at 675 °C for 1 h can cause the sensitization of grain boundaries (GBs). However, for forging 316L stainless steel, it was not found that the microscopic interface would accelerate the corrosion damage, and the grain size could only undergo sensitization after heating at 675 degrees for 24 h. Therefore, the interface between AM 316L and forging 316L steels has wide variations in terms of the effects on corrosion and sensitization phenomena. Research [11] found that traditional 316L steel has poorer resistance to intergranular corrosion compared to 316L steel manufactured by SLM. Through the study of SLM 316L steel, it was found that after sensitization treatment, numerous special grain boundaries and other structures with no Cr enrichment appeared in the SLM sample, thus avoiding local Cr depletion. On the other hand, related studies [12] suggest that the difference in the microstructure can promote the generation of a better passivation film for SLM 316L steel compared to forging stainless steel in a corrosion solution. The absence of sulfides and micro defect entanglement near the impurities in SLM 316L steel results in a significantly greater corrosion resistance of SLM 316L stainless steel than forging samples. In addition, when SLM 316L steel was heated at lower temperatures (below 650 °C), the grain size increased, and more $MnCr_2O_4$ inclusions were formed when treated at higher temperatures (1100 °C) [13]. For the SLM steel, the lower-temperature heat treatment improved the polarization resistance and did not change the pit corrosion mechanism, while the higher-temperature heat treatment reduced the polarization resistance but altered the corrosion resistance mechanism. It can be seen that a considerable amount of work has been carried out in the research of AM materials.

In the articles mentioned above, it has been proposed that the microstructures, such as fabricating-induced defects, GBs, and MPBs, in SLM steel influence the local corrosion behavior. However, due to the diversity of AM alloys, there are still many differences in the study of their local corrosion performance. In addition, the correlation in the local corrosion behavior between forging steel and SLM steel has not been fully explained. Currently, few studies have revealed the relationship between intergranular corrosion and pit corrosion, and further in-depth research is needed. Hence, in order to widely apply forging and SLM steels, it is extremely important to reveal their local corrosion behavior theory.

In this paper, the local corrosion behavior of forging and SLM 304 stainless steels was investigated by electrochemical tests. Intergranular corrosion and double-loop electrochemical potentiodynamic reactivation (DL-EPR) experiments were performed to study the sensitization behavior; also, a dynamic polarization test was conducted to investigate the pit corrosion. The degree of sensitization (DOS) and pit corrosion behavior of the forging and SLM steels were compared, and the relationship between the intergranular and pit corrosion was analyzed based on structural characterization and passivation film analysis.

2. Experiments and Details

The elemental compositions of the forging and SLM 304 steels involved are shown in Table 1. Before all the experiments, the forging 304 steel was subjected to 1 h of heat annealing treatment at 1050 °C and then quenched in water. The SLM 304 steel plate

was printed by an EOS M290 metal 3D printing device produced in Germany. As shown in Figure 1a, the size of the printed 304 steel metal powder ranged from 20 to 40 μm. When printing the sheet, the sheet was built vertically, and the laser scanning direction rotated approximately 67° between two consecutive layers. SLM operates in a powder bed, building components layer-by-layer by rastering a high-powered laser directed by a computer-aided design model. After each intermediate layer was completed, the printing stage was gradually lowered, and then another metal powder layer was added through the working arm [14]. The scanning speed of the laser was 6.7–8.3 mm/s, and the laser power was 2.8–3.0 kW. To prevent or reduce oxidation, the printing process was carried out under an inert gas atmosphere of argon while keeping the printing chamber under a positive pressure [15,16]. The printing method sketch map is displayed in Figure 1b. Finally, a printed board was obtained through the printing equipment (length 85 mm, width 25 mm, thickness 6 mm). The test sample was cut from the printed board, and the test surface of the sample is shown in Figure 1b. To sensitize the stainless steels, the forging and SLM 304 steels were heated at 650 °C for 9 h in an atmosphere furnace and then cooled in the furnace. This study included four types of samples: forging 304 steel, sensitized forging 304 steel, SLM 304 steel, and sensitized SLM 304 steel, represented as forging, forging + ST, SLM, and SLM + ST.

Table 1. Elemental constituents of the forging and SLM 304 steels (wt.%).

	Cr	Ni	Mn	Si	N	S	P	C	Fe
Forging	18.09	8.06	1.13	0.33	0.05	0.02	0.04	0.07	Bal.
SLM	18.19	8.61	1.12	0.36	0.06	0.02	0.02	0.08	Bal.

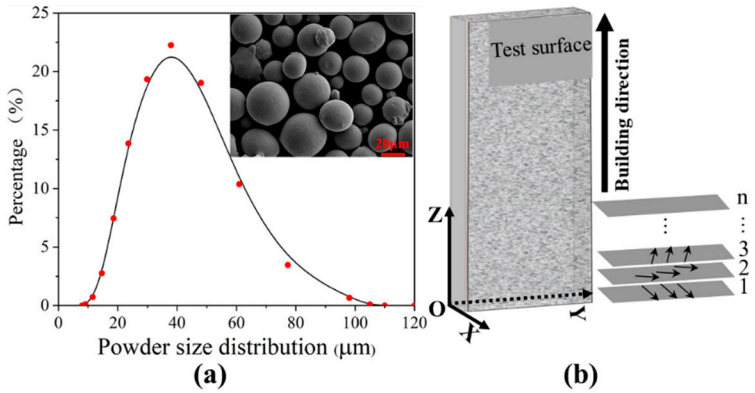

Figure 1. (**a**) Powder size distribution of SLM 304 steel; (**b**) the printing method sketch map.

When conducting the electrochemical experiments, the back of the stainless-steel material obtained was welded with an insulated copper line and embedded in a plastic tube using epoxy jaffaite to make a sample with a testing area of 1 cm^2. Then, the surface of the sample was gradually polished using SiC sandpaper with a particle size of 180–2000, and, finally, a 1 μ diamond slurry was used at a certain scale to grind to obtain a smooth-surfaced sample. Before conducting the electrochemical experiment, the sample was cleaned using ultrasound and blow-dried with air. During the intergranular corrosion test, the sample was subjected to a 10% oxalic acid solution at 25 ± 1 °C, and the experimental current was about 1 Acm^{-2} for 2 min (anode: the test sample; cathode: the steel plate). After the corrosion was completed, the sample was cleaned with flowing water, dried with a hair dryer, and then observed under an optical microscope (OM). In addition, DL-EPR and dynamic polarization experiments were conducted using an IviumStat electrochemistry device to investigate the DOS and pitting behavior of the forging and SLM stainless steels, respectively. The electrochemical workstation had three electrodes, where the stainless-steel sample was the working electrode, the platinum sheet was the counter electrode, and the 232 saturated calomel electrode (SCE) was the reference electrode (0.244 V relative to

standard hydrogen electrodes at 25 °C). All the potentials obtained from the experiment were based on SCE as the standard. The experiment used a constant-temperature circulating water bath to maintain a temperature of 25 ± 1 °C. Meanwhile, before the experiment, the stainless-steel sample was placed in the solution for about 10 min to make the experiment more stable. In the DL-EPR experiment, the solution medium was obtained by dissolving 0.5 M H_2SO_4 and 0.01 M KSCN chemical reagents in distilled water. The potential was scanned from (−0.400) V_{SCE} to (+0.400) V_{SCE} at a scanning rate of +0.2 mV/s and then scanned in reverse to the initial potential. Then, the DOS value was obtained by calculating the percentage (I_r/I_a) of the peak reactivation current (I_r) and peak activation current (I_a). In addition, the dynamic polarization experiment was conducted in a 0.9% NaCl electrolyte solution at 25 ±1 °C, and the experiment scanned from (−1.0) V_{SCE} to (+1.0) V_{SCE} at a rate of (+0.2) mV/s, obtaining the dynamic polarization curve. Each experiment was repeated at least ten times to ensure its reliability.

Furthermore, the microstructure, element content, sample surface, and oxide film of the 304 steel were analyzed and studied employing OM, scanning electron microscopy (SEM), electron backscatter diffraction (EBSD), SEM-EDS (energy dispersive X-ray spectroscopy), and X-ray photoelectron spectroscopy (XPS). The acceleration voltage for the EBSD testing was 20 kV, the scanning speed was 636.24 Hz, and each step length was 0.75 μm. The electron energy of the XPS test electron source was 2000 eV, with an energy half width of 0.4 eV. The minimum beam spot diameter was about 1 mm, and the maximum output current was about 64 μA.

3. Results and Discussion

3.1. Structure Characteristics

The microstructure test samples of the forging 304 stainless steel were taken from smooth annealed sheets, which are displayed in Figure 2. The metallographic phase of the forging material was observed by electrochemical corrosion, as shown in Figure 2b. The grains of the forging 304 steel had an irregular polygon morphology, and the GBs were straight, which is a typical morphology of traditional stainless steel. In addition, some twinning crystals were generated between the grains. The EBSD inverse-pole figure (IPF) of the forging 304 steel showed that the grain orientation was uniformly distributed in the traditional 304 steel, and no preferred orientation was observed (Figure 2c). As shown in Figure 2, the grains of the forging 304 samples were irregular polygons in the IPF, and their size was about 45~60 μm. Moreover, the GB distribution of the forging and SLM 304 stainless steels was observed by EBSD, and the results are shown in Figures 2d and 3d. In the GB distribution pictures, a high-angle GB (HAGB) with an orientation difference of greater than 15° is displayed using black color, while a lower-angle GB (LAGB) with an orientation difference of less than 15° is displayed by using color. Figure 2d displays the distribution and number of HAGBs and LAGBs of the forging 304 steel. The low density of the LAGBs was not uniformly distributed around the HAGBs in the forging 304 steel, which occupied 61.1% of all the GBs. The calculated average misorientation angle for the forging 304 steel was 35.21°.

Compared to the forging 304 stainless steel, the surface of the SLM material was very rough, which was caused by the melting of the powder, as shown in Figure 3a. During SLM molding, a high-energy laser interacts with the powder bed to form multiple molten pools, and the local peak temperature can reach several thousand degrees [17–19]. The solidification trajectory and melt pool perpendicular to the construction direction in the SLM steel are shown in the metallographic phase in Figure 3b, and the average size of the fan-shaped melt pool was about 100 μm. SLM forming uses high-energy laser beams to selectively melt pre-laid thin layers of metal powder and then allowing them to solidify and form, and after layer-by-layer stacking, the material is obtained. The incremental layer-by-layer melting and solidification construction process of the metal powder causes the formation of typical fan-shaped melt pools [20]. The alternating direction of the melt pool is caused by continuously turning the high-energy laser during printing [21]. The

re-melting that occurs during the printing process can cause many overlapping printing trajectories and melt pools in the material.

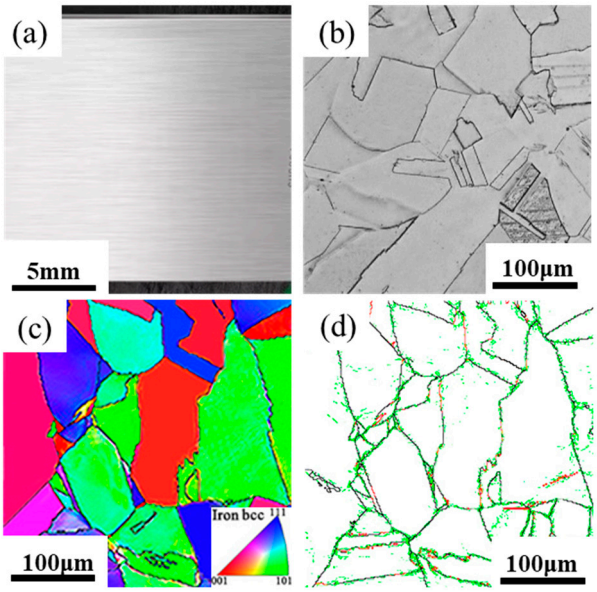

Figure 2. Microstructural characterization of forging 304 stainless steel. ((**a**): Solution-annealed material; (**b**): metallography; (**c**): grains and grain orientation; (**d**): grain boundary).

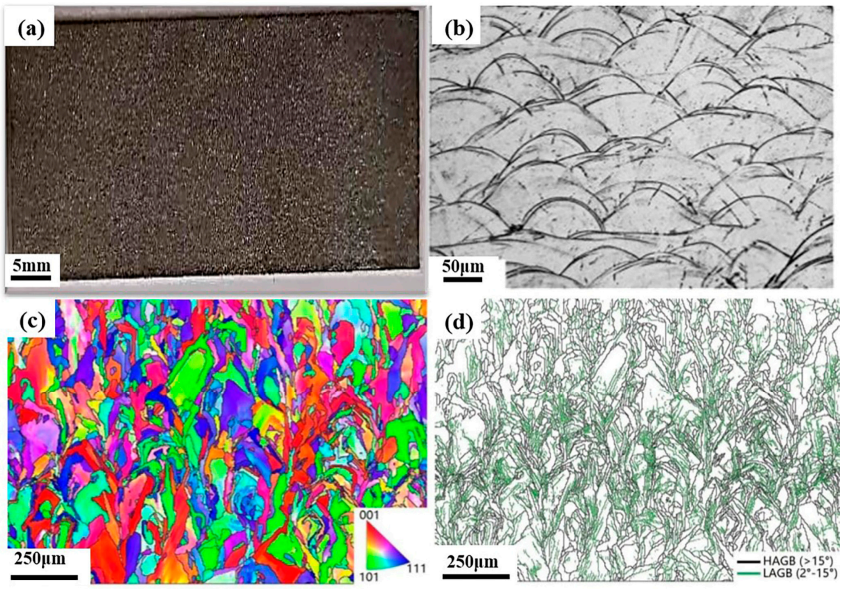

Figure 3. Microstructural characterization of SLM 304 stainless steel. ((**a**): Print material; (**b**): molten pool; (**c**): grains and grain orientation; (**d**): grain boundary).

As shown in Figure 3c, which shows the IPF of the SLM 304 steel, it can be seen that there was no preferred orientation phenomenon in the original printed SLM steel. The grains of the SLM steel had a unique ripple shape, which was significantly different from the facet shape in the traditional steel. The GBs diagram in Figure 3d shows that the morphology of the SLM steel grains was irregular and curved, which made the IPF present a strip shape. In the traditional 304 steel, the grain size and orientation were very uneven, but the distribution was relatively regular. The statistics show that the average grain size of the SLM 304 steel was about 58.6 μm. The above characteristics of the SLM 304 steel were caused by the unique scanning strategy in the SLM process. Figure 3d shows the distribution and number of HAGBs and LAGBs of the SLM 304 steel. The calculated

average misorientation angle was 13.83° for the SLM 304 steel. The high density of LAGBs was not uniformly distributed in the SLM 304 steel, which occupied 49.6% of the total. LAGBs with an orientation difference between 2° and 15° are considered to be composed of dislocations. Research has shown that the interface structure in SLM samples seriously affects their corrosion properties [22].

3.2. Passivation Film Characteristic Tests

The ability to resist corrosion of a material has a close relationship with the characteristics of its surface facial film [23]. In order to investigate the ability to resist corrosion of the forging and SLM 304 steels in depth, the film on the surface of the forging and SLM 304 steels was studied through XPS experiments. The results of the XPS test analysis are displayed in Figure 4, showing the peaks of the Cr, Fe, Ni, and O chemical elements detected. Among them, only the metallic element Ni was identified in the passivation film, with a binding energy of 853.0 eV, and no oxidized Ni element was identified. For the Fe, Cr, and O elements in the membrane, this article is based on Shirley's principle [24,25] and deconvolutes the spectrum based on the binding energy of the chemical element background subtraction. Further referring to the elemental spectra in the relevant literature [26,27], the elements tested in this study were subjected to peak separation to obtain their different component compositions. Meanwhile, the possible components obtained from the passivation film complied with the standards in the XPS manual [28,29].

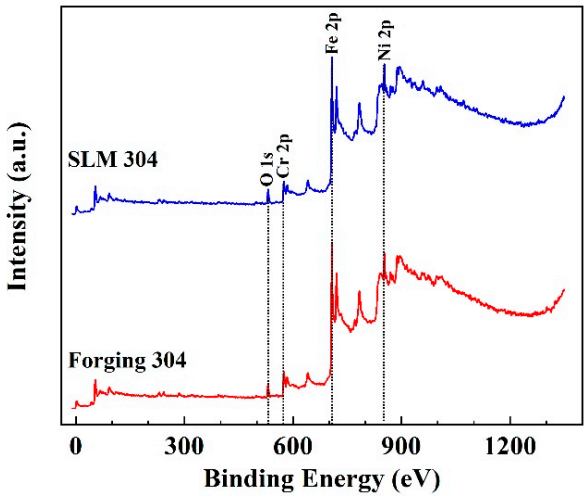

Figure 4. Element analysis of XPS tests for the passivation film of forging and SLM 304 steels.

Figure 5 displays the XPS results of Fe $2p_{3/2}$, Cr $2p_{3/2}$, and O 1s of the facial films of the forging and SLM 304 steels. More information about the composition of the facial films is shown in Table 2. As shown in Figure 5a, Fe $2p_{3/2}$ can be considered to be composed of four components: Fe_{met} (metallic form), Fe_3O_4, FeO, and FeOOH. The details of the positions of these components are displayed in Table 2. Observing the intensity of the four components, it is thus clear that the intensity of Fe_{met} was significantly higher than the peak intensity of the other three components. In addition, Cr $2p_{3/2}$ can be considered to be composed of Cr_{met}, Cr_2O_3, and $Cr(OH)_3$ components, as shown in Figure 5b, and the details of their component positions are shown in Table 2. According to relevant research results [30], the generation of more chromium oxides in the passivation film will optimize the stability and reduce the passive current of the material. The content fraction of the Cr_2O_3 composition within the passivation film of the forging and SLM 304 steels was 34.14% and 35.09% according to calculations, respectively. Moreover, the ratio of Cr/Fe in the facial film composition of stainless steel can reflect its passivation ability. Generally, the larger the ratio, the higher the ability to resist corrosion of the facial film [31]. The Cr/Fe ratio of the SLM 304 steel was 0.21, which was higher than that of the forging 304 steel by 0.18, indicating that the passivation ability of the SLM 304 was greater than that

of the forging 304 steel. On the other hand, O^{2-} or OH^{-} on the surface of steel plays a role in connecting metal ions, and compared with hydroxides, oxides are more conducive to increasing the ability to resist corrosion of the material [32]. As shown in Figure 5c, the O 1s compositions of the facial films of the forging and SLM 304 steels were analyzed. O 1s consists of three constituents, namely O^{2-}, OH^{-}, and H_2O, and their positions are shown in Table 2. In addition, O^{2-} is related to the components of Cr_20_3, Fe_3O_4, and FeO, while OH^{-} is related to the components of $Cr(OH)_3$ and FeOOH. Simultaneously, it can be observed that the strength of O^{2-} is much higher than that of OH^{-}. The oxide proportion of the passivation film of the SLM 304 steel was larger than that of the forging 304 steel, which would cause the SLM 304 steel to have a higher ability to resist corrosion. To summarize, the ability to resist corrosion of the passivation film of the SLM 304 steel was greater than that of the forging steel, which may affect its corrosion resistance.

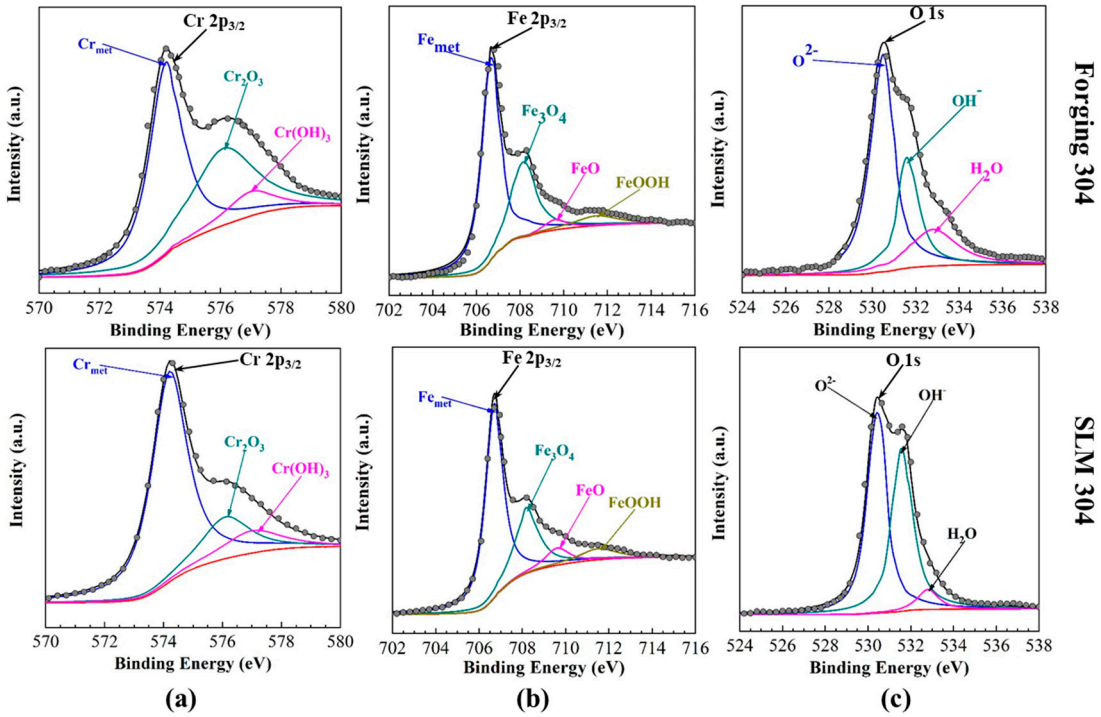

Figure 5. XPS spectra of Fe $2p_{3/2}$ (**a**), Cr $2p_{3/2}$ (**b**), and O 1s (**c**) peaks of the passivation films of forging and SLM 304 steels.

Table 2. XPS analysis of the properties of the passivation films of forging and SLM 304 steels.

Element	Component	Position eV	Component Proportion	
			Forging 304	SLM 304
Fe	FeOOH	711.5	20.01	22.14
	FeO	709.6	23.64	24.13
	Fe_3O_4	708.2	26.52	26.16
	Fe_{met}	706.7	29.83	27.57
Cr	$Cr(OH)_3$	577.0	29.65	30.02
	Cr_2O_3	576.1	34.14	35.09
	Cr_{met}	574.2	36.21	34.89
O	H_2O	533.5	31.38	32.19
	OH^{-}	532.1	32.67	33.38
	O^{2-}	530.4	35.95	34.43
Cr/Fe			0.18	0.21

3.3. Intergranular Corrosion Tests

The surface morphologies of the forging and SLM 304 steels with and without sensitization treatment after the intergranular corrosion measurements are presented in Figure 6. As can be seen, the intergranular corrosion characteristics of the 304 steels with or without sensitization treatment were very different under the same test conditions. As can be seen in Figure 6a,a1, the GB of the forging sample was slightly corroded, and the outlines of some grains were fuzzy. However, significant deep and wide corrosion grooves appeared in the sensitized sample of the forging + ST sample. The GBs of the forging + ST sample were seriously corroded compared with the forging sample. There is no doubt that the degree of GB corrosion of the forging 304 steel was seriously aggravated after the sensitization treatment. On the other hand, regular melt pool boundaries appeared in the SLM sample after the intergranular corrosion, but GBs did not, as shown in Figure 6c. Also, the melt pool boundaries were slightly corroded, as presented in a locally enlarged view in Figure 6c1. After the sensitization treatment, many irregular grains were found in the SLM + ST sample, as shown in Figure 6d. The GBs of the SLM + ST sample were seriously corroded, while the melt pool boundaries were not. In addition, the intergranular structure of the SLM + ST sample was more severely corroded compared with the forging + ST sample, as shown in Figure 6a1,d1. These results indicate that SLM technology can improve the sensitization of 304 stainless steel.

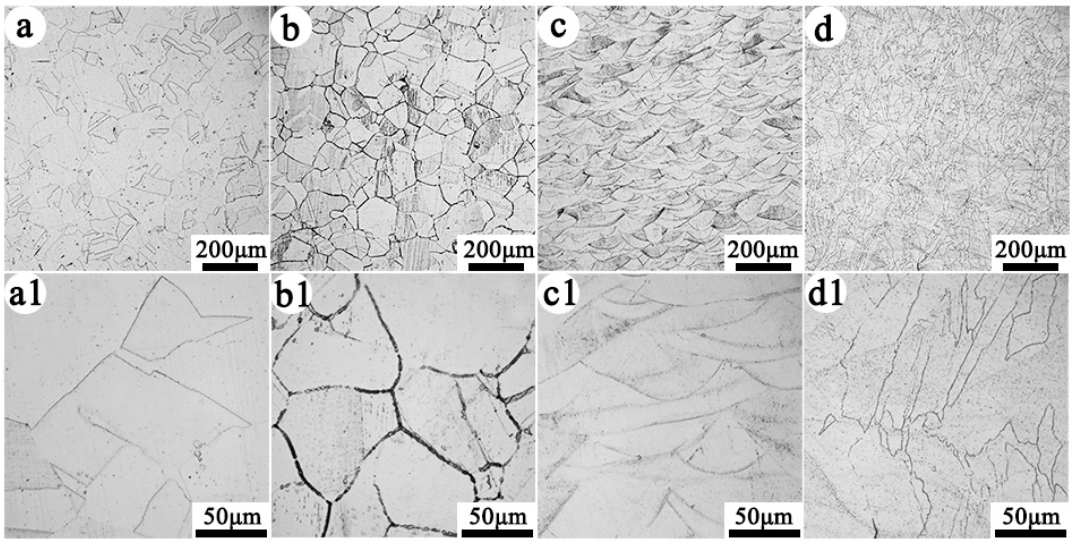

Figure 6. Surface morphologies of forging and SLM 304 steels with and without sensitization treatment after intergranular corrosion tests. (**a**,**a1**): Forging, (**b**,**b1**) forging +ST, (**c**,**c1**) SLM, (**d**,**d1**) SLM + ST; (**a1**–**d1**): local enlarged view of the corresponding sample.

The element Cr is an important element that affects the sensitization properties of metal materials [33]. The Cr content in the materials near the GBs of the forging and SLM 304 steels after the sensitization treatment was studied by SEM-EDS, and the results are shown in Figure 7. It is clear that the Cr element content of the forging + ST sample near the GBs (about 15.82%) was less than in the SLM + ST sample (about 20.16%). This conclusion may affect the sensitivity resistance of the GBs of the two types of steel. Research has shown that the carbon in austenitic stainless steel is generally completely dissolved at high temperatures [34]. When it is cooled to room temperature, the carbon exists in the matrix in a supersaturated state. When it is reheated to an appropriate temperature, i.e., the sensitization temperature, and maintained for sufficient time, the carbon will precipitate in the form of carbide. Common types of carbide include MC, M6C, and especially M23C6, which usually form at the phase boundary and GBs of stainless steel. In other words, a lot of carbides will be produced in stainless steel when it is sensitized in a specific temperature range. The precipitation of M23C6 rich in Cr will lead to a decrease in the Cr content in

its vicinity. Due to the extremely slow diffusion of Cr, the Cr in this area cannot be fully supplemented, forming a Cr-poor area, which reduces the ability to resist corrosion of the materials [35]. Here, the forging and SLM 304 steels were treated with sensitization, which caused an impoverishment of the Cr near the GBs, resulting in a poor ability to resist corrosion of the GBs. The above conclusions indicated that the Cr percentage of the forging + ST sample near the GBs was less than that of the SLM + ST sample; therefore, the sensitivity resistance of the GB of the forging + ST 304 steel was worse than that of the SLM + ST 304 steel.

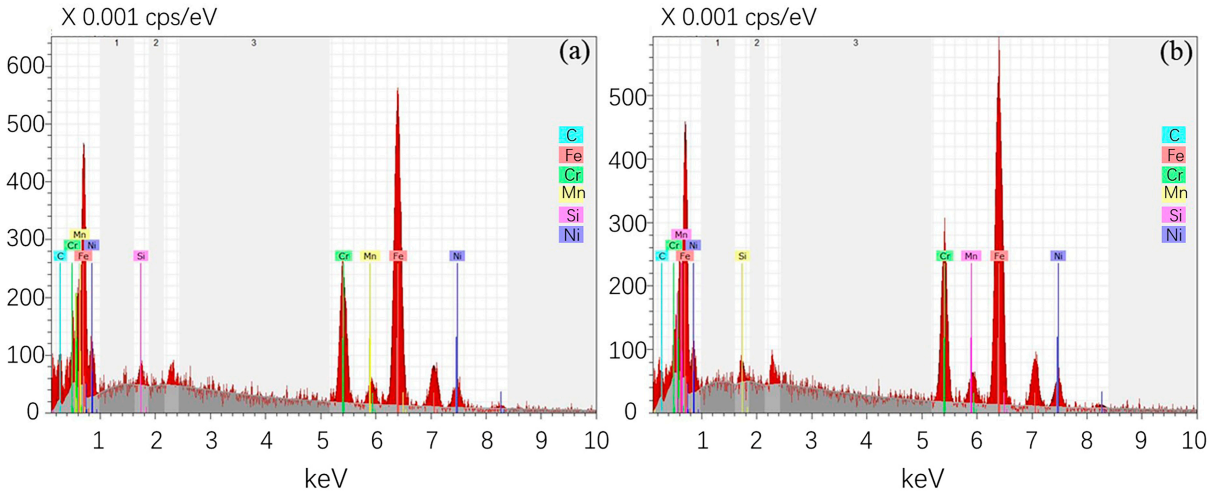

Figure 7. SEM-EDS results from near grain boundaries after sensitization treatment of forging and SLM 304 steels. (**a**) Forging + ST, (**b**) SLM + ST.

3.4. Double-Loop Electrochemical Potentiodynamic Reactivation

For all the experimental curves, the higher I_a value was caused by the dissipating of chemical elements in the material. Then, the I_a value dropped to a lower passivation current density before running to the presupposed reverse potential of +400 mV. The surface passivation film can be seen as a barrier between metals and the environment, reducing the dissolution rate of metals. During the reverse scanning process, an incomplete passivation behavior during the forward scanning process can cause intergranular corrosion behavior, which can reflect the degree of Cr element loss caused by chromium carbide precipitation in steel materials. In the experiment of the 304 steel, corrosion occurred at the grain boundaries and interdendritic boundaries in the steel material during the forward scanning of the δ-ferrite or σ areas with less Cr element in the vicinity. During the reverse scanning process, corrosion damage occurred due to incomplete passivation during the forward scanning process, which revealed the formation of chromium carbide precipitates near the grain boundaries of the steel materials [36]. In addition, the I_r value revealed in the DL-EPR experiment that the material was passivated due to the consumption of Cr element, resulting in a lower value of I_r than the value of I_a [37].

As shown in Figure 8, the forging and SLM 304 steels did not reflect the sensitization behavior, a large arc appeared in the curve when scanning in reverse in the solution, and the I_r and I_a values were similar. However, the forging + ST and SLM + ST samples presented an increase in I_r, especially the SLM + ST sample. This indicated that the forging + ST sample experienced serious sensitization; also, the SLM + ST sample was slightly sensitized. Table 3 displays the detailed values extracted from the DL-EPR results of the forging and SLM 304 steels. The forging and SLM 304 steels did not show a reactivation peak; therefore, there was no DOS value. The DOS value of the forging + ST sample (26.91%) was somewhat larger than that of the SLM + ST sample (2.51%), revealing severe intergranular corrosion in the forging + ST sample. That is to say, severe grain boundary corrosion occurred in the forging 304 steel during the heat treatment at a temperature of 650 °C for 8 h, while there was a slight presence of it in the SLM 304 steel. This conclusion was also confirmed by

the SEM-EDS results shown in Figure 5. It is obvious that the forging 304 steel had a high degree of sensitization caused by the heat treatment, while the SLM 304 steel was slightly sensitized. Therefore, SLM 304 steel has a stronger ability to resist sensitization compared with forging 304 steel. Thus, SLM technology can improve the ability of 304 steel to resist intergranular corrosion.

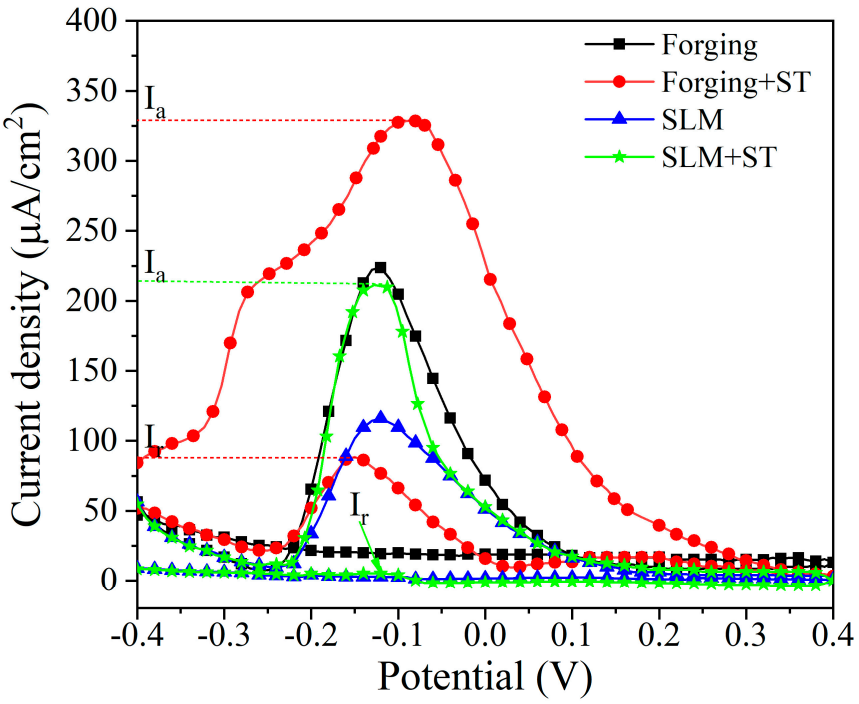

Figure 8. DL-EPR diagrams of forging and SLM 304 steels with and without sensitization treatment.

Table 3. DOS values and details of the DL-EPR curves.

Samples	I_a (μm/cm²)	I_r (μm/cm²)	%DOS (I_r/I_a)
Forging	223.78 ± 8.4	No reactivation peak	No
Forging + ST	328.43 ± 10.23	88.37 ± 2.73	26.91 ± 1.72
SLM	111.40 ± 3.26	No reactivation peak	No
SLM + ST	174.23 ± 2.92	6.17 ± 0.24	2.51 ± 0.29

3.5. Dynamic Polarization Experiments

The dynamic polarization results of the forging and SLM 304 steels with and without sensitization treatment are displayed in Figure 9. The details of the relevant electrochemical parameters of the polarization results are shown in Table 4 (I_c: corrosion current density, E_c: corrosion potential, E_p: pit corrosion potential, I_p: passivation current density). The E_p value was determined as the potential at which the current obviously increased and continued to rise, and the I_p value was obtained from the middle of the passive region.

Regarding the results, the E_p value of 0.434 V_{SCE} for the SLM sample was much higher than that of 0.176 V_{SCE} for the forging sample. Thus, the ability to resist corrosion of the SLM 304 steel was greater than that of the forging 304 steel. SLM technology can improve the ability to resist pit corrosion of 304 steel, which is of great value in the application of steel materials. Moreover, the E_p value of −0.038 V_{SCE} for the forging + ST sample was much lower than that of 0.176 V_{SCE} for the forging sample. Hence, the ability to resist pit corrosion of the forging 304 steel was obviously weakened after the sensitization. The I_p value of the forging 304 steel increased from 2.565 μA cm^{-2} (forging sample) to 7.462 μA cm^{-2} (forging + ST sample) after the sensitization; the ΔE value decreased from

0.341 V_{SCE} (forging sample) to 0.334 V_{SCE} (forging + ST sample). The I_p and ΔE values can represent the characteristics of the passivation films of metals [17,37,38]. Generally, the smaller the I_p value or the higher the ΔE value of steel materials, the slower the corrosion rate and the better the quality of the passivation film on the material. It is thus clear that the pit corrosion of the forging 304 steel was significantly deteriorated by the sensitization, and the stabilization of the passivation film was weakened.

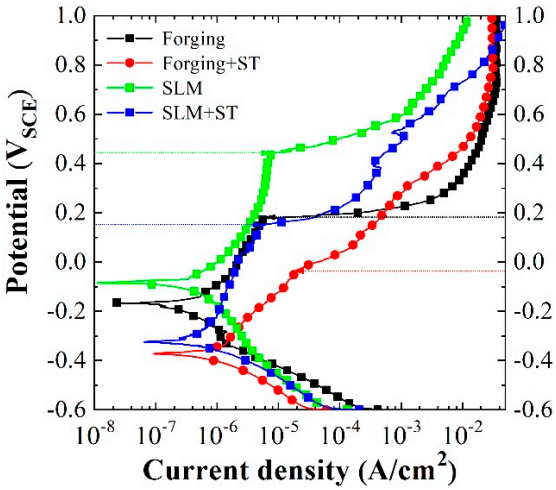

Figure 9. Dynamic polarization plots of forging and SLM 304 steels with and without sensitization treatment.

Table 4. Electrochemical parameters of forging and SLM 304 steels with and without sensitization treatment in 0.9% NaCl solution at 25 ± 1 °C.

Samples	E_p (V_{SCE})	I_p (μA cm^{-2})	E_c (V_{SCE})	I_c (nA cm^{-2})
Forging	0.176 ± 0.003	2.565 ± 0.014	−0.165 ± 0.004	23.147 ± 0.115
Forging + ST	−0.038 ± 0.001	7.462 ± 0.023	−0.372 ± 0.005	83.625 ± 0.127
SLM	0.434 ± 0.008	2.363 ± 0.019	−0.085 ± 0.001	8.696 ± 0.014
SLM + ST	0.147 ± 0.001	2.567 ± 0.016	−0.328 ± 0.003	42.118 ± 0.038

For the SLM 304 steel, the E_p value of 0.147 V_{SCE} for the SLM + ST sample was much lower than that of 0.434 V_{SCE} for the SLM sample. Therefore, the ability to resist pit corrosion of the SLM 304 steel also deteriorated after the sensitization. In addition, the I_p value of the SLM sample (2.363 μA cm^{-2}) was lower than that of the SLM + ST sample (2.567 μA cm^{-2}). Ultimately, the ability to resist pit corrosion of the SLM 304 steel was also weakened by the sensitization, which was in agreement with the forging 304 steel.

After the dynamic polarization tests, the corrosion pits of the forging and SLM 304 steel samples were recorded. The statistical ratio of the number of corrosion pits of the samples after the same number of dynamic polarization experiments is shown in Figure 10. Analyzing the above experiment, most of the corrosion pits occurred at the GBs in the forging samples; the percentage of the corrosion pits that formed near the GBs in the forging + ST sample was much more than in the forging sample. This reflects that the GBs of the sensitized forging 304 steel were more likely to induce pit corrosion. For the SLM 304 steels, the percentage of corrosion pits that occurred at the melt pool boundaries was much higher than the GBs for the SLM sample, while it was the opposite for the SLM + ST sample. After the sensitization treatment, the ability to resist corrosion of the GBs of the SLM steel was weakened, resulting in pit corrosion being more likely to be induced at the GBs.

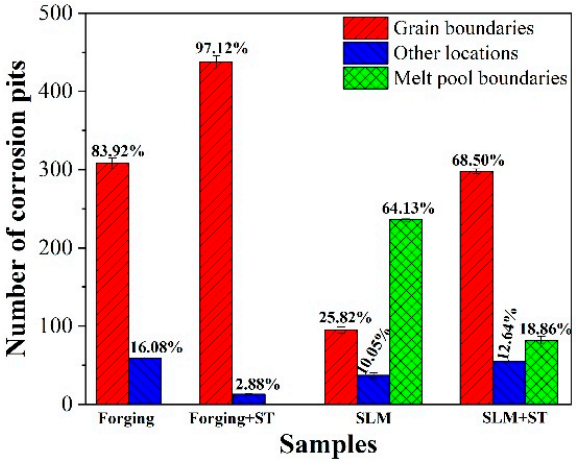

Figure 10. Statistics of corrosion pits for forging and SLM 304 steels with and without sensitization treatment after the dynamic polarization tests.

The surface morphologies of the forging and SLM 304 steels during the dynamic polarization experiments were observed, as shown in Figure 11. A large number of corrosion pits formed near the GBs in the forging 304 steel, especially in the forging + ST sample (Figure 9b). In the SLM sample, the melt pool boundaries were more seriously corroded, and some corrosion pits occurred at them, while the GBs were slightly corroded (Figure 11c). For the SLM + ST sample, the GB was seriously corroded, and plenty of corrosion pits appeared at the GB, while the molten pool boundary was not (Figure 11d). Therefore, pit corrosion easily occurred in the SLM 304 steel at the MPBs and GBs, while it occurred more easily in the forging 304 steel at the GBs. The corrosion degree of the MPBs of the SLM steel weakened, and the GB corrosion was more severe after the sensitization treatment, which led to more severe pit corrosion at the GBs.

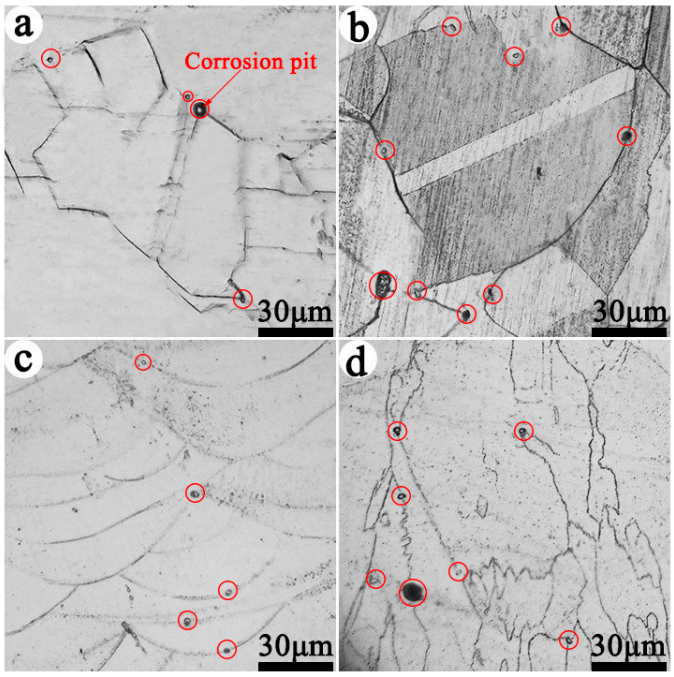

Figure 11. Optical images of forging and SLM 304 steels during the dynamic polarization tests. ((**a**): Forging; (**b**): forging + ST; (**c**): SLM; (**d**): SLM + ST).

According to the research results, the structures of the forging and SLM 304 steels were significantly different, which affected the pit and sensitization resistance. The corrosion

pits of the 304 steel were preferentially initiated at the interface. Chemical components such as C, O, and Si near MPBs have a strong activity, which makes the MPBs sensitive to corrosion [38]. When MPBs and GBs are present in SLM steels, the deepening of the corrosion at the MPBs will reduce the corrosion at the GBs, making it easier for pitting corrosion to form at the MPBs. When only GBs exist in steel materials, the sensitivity of the GBs to corrosion varies greatly due to their structure and distribution. Compared to the original matrix of the materials within grains, the GBs are easily damaged. The disordered arrangement of the atomic structures at the GBs is a linear defect that is more susceptible to corrosion and damage. On the other hand, the structure of GBs can lead to a decrease in the conductivity of steel, resulting in a decrease in its passivation ability and ultimately a decrease in its ability to resist corrosion [39,40]. The above research results, as shown in Figure 6, confirm that GBs in steel materials have poor resistance to corrosion in corrosive environments. Corrosion pits are more likely to form at grain boundaries, and the damaged area of the corrosion pits gradually grows, ultimately leading to severe material damage. After the sensitization treatment of the 304 steel, the ability of the GBs to resist corrosion was significantly reduced, resulting in pitting corrosion more easily forming and growing at the grain boundaries, which weakened the corrosion resistance of 304 steel.

Moreover, before the sensitization treatment of the SLM 304 steel, the corrosion at the MPBs was more severe than at the GBs, and corrosion pits preferentially formed at the MPBs; after the sensitization treatment, the corrosion at the GBs of the stainless steel intensified, and pit corrosion preferentially formed at the GBs. The GB corrosion resistance of the forging and SLM 304 steels significantly decreased after the sensitization treatment, resulting in a significant decrease in the pit corrosion resistance of the 304 steel. However, the unique MPB and GB structures of the SLM 304 stainless steel made its sensitivity resistance significantly higher than that of the forging 304 stainless steel. Moreover, when the SLM 304 steel was sensitized, its internal MPBs disappeared, the pit corrosion resistance of the GBs decreased significantly, and a large number of pits easily formed at the GBs, which reduced the corrosion resistance of the SLM 304 steel. Moreover, the resistance to corrosion of the passivation film of the SLM 304 steel was greater than that of the forging steel. The coupling effect of these different structures and the passivation film decides the pit and sensitization resistance of forging and SLM 304 steels. Clarifying the corrosion mechanism of forging and SLM steels is of great significance for scientific research and the widespread use of SLM technology.

4. Conclusions

The sensitization characteristics and pit corrosion properties of forging and SLM 304 steels were studied and analyzed through electrochemical experiments, microstructure observation, and an analysis of the passivation film characteristics. The conclusions are as follows:

(1) The ability to resist sensitization of the SLM 304 steel was greater than that of the forging 304 steel at a temperature of 650 °C for 9 h. SLM technology improves the ability to resist sensitization of 304 steel.
(2) The pit corrosion resistance of the forging and SLM 304 steels was weakened by the sensitization treatment, while the pit corrosion resistance of the SLM 304 steel was greater than that of the forging steel. SLM technology optimizes the ability to resist pit corrosion of 304 steel.
(3) The ability to resist corrosion of the passivation film of the SLM 304 steel was greater than that of the forging 304 steel, which affected its corrosion resistance.
(4) Corrosion pits were more easily generated at the interface of the forging and SLM 304 steels. The grain boundary corrosion of the SLM 304 steel intensified, while the melt pool boundary corrosion weakened after the sensitization treatment, resulting in a decrease in pit corrosion resistance.

Author Contributions: Methodology, Y.C.; Investigation, H.T.; Resources, Z.T., Y.H. and M.D.; Writing—original draft, H.T.; Writing—review and editing, H.T. All authors have read and agreed to the published version of the manuscript.

Funding: This research was funded by the "Pioneer" and "Leading Goose" R&D Program of Zhejiang (2022C01070 and 2023C01156), Key Laboratory for Technology in Rural Water Management of Zhejiang Province (ZJWEU-RWM-20200304B), and Nanxun Scholars Program for Young Scholars of ZJWEU (RC2022021035).

Institutional Review Board Statement: Not applicable.

Informed Consent Statement: Not applicable.

Data Availability Statement: All data that support the findings of this study are included within the article.

Conflicts of Interest: The authors declare that they have no known competing financial interests or personal relationships that could have appeared to influence the work reported in this paper. The authors declare that the research did not involve human participants or animals.

References

1. Kanko, J.A.; Sibley, A.P.; Fraser, J.M. In situ morphology based defect detection of selective laser melting through inline coherent imaging. *J. Mater. Process. Technol.* **2016**, *231*, 488–500. [CrossRef]
2. Qi, K.; Chang, T.; Shi, Z.; Gu, J.; Li, T.; Li, R. Investigation on electron beam welding of dissimilar wrought/selective laser melting aisi 304 stainless steel plates. *Int. J. Mod. Phys. B* **2022**, *9*, 36. [CrossRef]
3. Wang, X.J.; Xu, S.; Zhou, S.W.; Martin, L.; Peter, C.; Qian, M.; Mlian, B.; Xie, Y.M. Topological design and additive manufacturing of porous metals for bone. *Biomaterials* **2016**, *83*, 127–141. [CrossRef] [PubMed]
4. Song, X.P.; Huang, J.K.; Fan, D. Review of functionally graded materials processed by additive manufacturing. *China Weld.* **2023**, *32*, 41–50.
5. Wang, R.; Wang, J.; Lei, L.M.; Yu, S.; Hu, T.; Shuai, S.S.; Xu, S.Z.; Cao, Z.H.; Li, X.P.; Chen, C.Y.; et al. Laser additive manufacturing of strong and ductile Al-12Si alloy under static magnetic field. *Mate. Sci. Technol.* **2023**, *163*, 101–112. [CrossRef]
6. Reichardt, A.; Shapiro, A.A.; Otis, R.; Dillon, P.R.; Borgonia, J.P.; McEnerney, B.W.; Hosemann, P.; Beese, A.M. Advances in additive manufacturing of metal-based functionally graded materials. *Int. Mater. Rev.* **2020**, *66*, 1–29. [CrossRef]
7. Bertocco, A.; Esposito, L.; Aurino, A.; Borrelli, D.; Caraviello, A. Influence of SLM parameters on the compressive behaviour of lattice structures in 17-4PH stainless steel. *IOP Conf. Ser. Mater. Sci. Eng.* **2021**, *1038*, 012035. [CrossRef]
8. Xiao, Q.; Chen, J.; Lee, H.B.; Jang, C.; Jang, K. Effect of heat treatment on corrosion behaviour of additively manufactured 316L stainless steel in high-temperature water. *Corros. Sci.* **2023**, *210*, 110830. [CrossRef]
9. Yang, J.J.; Wang, Y.; Li, F.Z.; Huang, W.P.; Jing, G.Y.; Wang, Z.M.; Zeng, X.Y. Weldability, microstructure and mechanical properties of laser-welded selective laser melted 304 stainless steel joints. *Mater. Sci. Technol.* **2019**, *35*, 1817–1824. [CrossRef]
10. Macatangay, D.A.; Thomas, S.; Birbilis, N.; Kelly, R.G. Unexpected interface corrosion and sensitization susceptibility in additively manufactured austenitic stainless steel. *J. Sc. Eng.* **2018**, *74*, 153–157. [CrossRef]
11. Laleha, M.; Hughes, A.E.; Xua, W.; Haghdadi, N.; Wang, K.; Cizek, P.; Gibson, I.; Tan, M.Y. On the unusual intergranular corrosion resistance of 316L stainless steel additively manufactured by selective laser melting. *Corros. Sci.* **2019**, *161*, 108189. [CrossRef]
12. Man, C.; Dong, C.F.; Liu, T.T.; Kong, D.C.; Wang, D.K.; Li, X.G. The enhancement of microstructure on the passive and pitting behaviors of selective laser melting 316L SS in simulated body fluid. *Appl. Surf. Sci.* **2019**, *467*, 193–205. [CrossRef]
13. Bedmar, J.; Garcia-Rodriguez, S.; Roldan, M.; Torres, B.; Rams, J. Effects of the heat treatment on the microstructure and corrosion behavior of 316 L stainless steel manufactured by laser powder bed fusion. *Corros. Sci.* **2022**, *209*, 110777. [CrossRef]
14. Shipley, H.; McDonnell, D.; Culleton, M.; Coull, R.; Lupoi, R.; O'Donnell, G.; Trimble, D. Optimisation of process parameters to address fundamental challenges during selective laser melting of Ti-6Al-4V: A review. *Int. J. Mach. Tools. Manuf.* **2018**, *128*, 1–20. [CrossRef]
15. Gokuldoss, P.K.; Kolla, S.; Eckert, J. Additive manufacturing processes: Selective laser melting, electron beam melting and binder jetting selection guidelines. *Materials* **2017**, *10*, 672. [CrossRef]
16. Bhavar, V.; Kattire, P.; Patil, V.; Khot, S.; Gujar, K.; Singh, R. A review on powder bed fusion technology of metal additive manufacturing. In *Additive Manufacturing Handbook, Proceedings of the 4th International Conference and Exhibition on Additive Manufacturing Technologies-AM-2014, Banglore, India, 1–2 September 2014*; CRC Press: Boca Raton, FL, USA, 2017; pp. 251–261.
17. Hooper, P.A. Melt pool temperature and cooling rates in laser powder bed fusion. *Addit. Manuf.* **2018**, *22*, 548–559. [CrossRef]
18. Calta, N.P.; Wang, J.; Kiss, A.M.; Martin, A.A.; Depond, P.J.; Guss, G.M.; Thampy, V.; Fong, A.Y.; Weker, J.N.; Stone, K.H.; et al. An instrument for in situ time-resolved X-ray imaging and diffraction of laser powder bed fusion additive manufacturing processes. *Rev. Sci. Instrum.* **2018**, *89*, 055101. [CrossRef]
19. Bidare, P.; Bitharas, I.; Ward, R.M.; Attallah, M.M.; Moore, A.J. Fluid and particle dynamics in laser powder bed fusion. *Acta Mater.* **2018**, *142*, 107–120. [CrossRef]

20. Lu, Z.; Zhang, C.; Fang, R.; Zhang, H.; Zhou, H.; Deng, N.; Guo, Z.; Gu, L. Microstructure evolution and corrosion behavior of the novel maraging stainless steel manufactured by selective laser melting. *Mater. Charact.* **2022**, *190*, 112078–112090. [CrossRef]
21. Casati, R.; Lemke, J.; Vedani, M. Microstructure and fracture behavior of 316L austenitic stainless steel produced by selective laser melting. *J. Mater. Sci. Technol.* **2016**, *32*, 738–744. [CrossRef]
22. Lu, H.F.; Wang, Z.; Cai, J.; Xu, X.; Luo, K.Y.; Wu, L.J.; Lu, L.Z. Effects of laser shock peening on the hot corrosion behaviour of the selective laser melted Ti6Al4V titanium alloy. *Corros. Sci.* **2021**, *188*, 109558. [CrossRef]
23. Ma, W.; Wang, H.; Wang, Y.; Neville, A. Hua Y Experimental and simulation studies of the effect of surface roughness on corrosion behaviour of x65 carbon steel under intermittent oil/water wetting. *Corros. Sci.* **2022**, *195*, 109947. [CrossRef]
24. Liu, C.T.; Wu, J.K. Influence of pH on the passivation behavior of 254SMO stainless steel in 3.5% NaCl solution. *Carros. Sci.* **2007**, *49*, 2198–2209. [CrossRef]
25. Shirley, D.A. High-resolution x-ray photoemission spectrum of the valence bands of gold. *Phys. Rev. B* **1972**, *5*, 4709–4714. [CrossRef]
26. Haupt, S.; Calinsk, C.; Collisi, I.U.; Hoppe, H.W.; Speckmann, D.; Strehblow, H.H.S. XPS and ISS examinations of electrode surface and passive layers with a specimen transfer in a closed system. *Surf. Lnterf. Anal.* **1986**, *9*, 357–365. [CrossRef]
27. Yang, J.; Zou, H.; Li, X.; Chen, J.; Liu, Y. Effects of Cr content on the corrosion behavior of porous Ni–Cr–Mo–Cu alloys in H_3PO_4 solution. *Mater. Res. Express* **2021**, *8*, 096522. [CrossRef]
28. Bhattarai, J. The corrosion behavior of sputter-deposited ternary Zr-(12-18) Cr-W alloys in 12M HCl solution. *Nepal. J. Sci. Technol.* **2010**, *26*, 103–108.
29. Hollander, J.M.; Jolly, W.L. X-ray Photoelectron spectroscopy. Handbook of applied solid state spectroscopy. *Acc. Chem. Res.* **1970**, *3*, 193–200. [CrossRef]
30. Wang, X.; Mercier, D.; Zanna, S.; Seyeux, A.; Perrière, L.; Laurent-Brocq, M. XPS study of the thermal stability of passivated NiCrFeCoMo multi-principal element alloy surfaces. *Surf. Interface Anal.* **2023**, *55*, 457–465. [CrossRef]
31. Malladi, S.B.A.; Tam, P.L.; Cao, Y.; Guo, S.; Nyborg, L. Corrosion behaviour of additively manufactured 316L and CoCrNi. *Surf. Interface Anal.* **2023**, *55*, 404–410. [CrossRef]
32. Wang, X.Z.; Luo, H.; Luo, J.L. Effects of hydrogen and stress on the electrochemical and passivation behaviour of 304 stainless steel in simulated PEMFC environment. *Electrochim. Acta* **2019**, *293*, 60–77. [CrossRef]
33. Vukkum, V.B.; Delvecchio, E.; Christudasjustus, J.; Storck, S.; Gupta, P.K. Intergranular corrosion of feedstock modified-additively manufactured stainless steel after sensitization corrosion. *J. Sci. Eng.* **2023**, *79*, 624–636. [CrossRef]
34. Shimada, M.; Kokawa, H.; Wang, Z.J.; Sato, Y.S. Arrest of intergranular corrosion in austenitic stainless steel by twin-induced grain boundary engineering. In Proceedings of the Asian Pacific Conference on Fracture and Strength and International Conference on Advanced Technology in Experimental Mechanics; The Japan Society of Mechanical Engineers: Tokyo, Japan, 2017; Volume 2, pp. 1036–1040.
35. Wang, J.X.; Shi, W.; Xiang, S.; Ballinger, R.G. Study of the corrosion behaviour of sensitized 904l austenitic stainless steel in Cl-solution. *Corros. Sci.* **2021**, *181*, 109234. [CrossRef]
36. Weng, K.C.; Chi, T.K.; Kin, H.L.; Cheng, Z.C. *Desensitization of Austenitic and Duplex Stainless Steels by Laser Surface Melting, Proceedings of the 4th Pacific International Conference on Applications of Lasers and Optics, Wuhan, China, 24 March 2010*; Laser Institute of America: Orlando, FL, USA; Volume 806, pp. 23–25.
37. Zhao, B.; Dai, Q.; Zhao, Z.J.; He, M.; Wang, L.X.; Zhang, G.H. Study on grain boundary sensitization in heat affected zone of austenitic stainless steel and its evaluation method. *Mater. Sci. Forum* **2022**, *1066*, 65–69. [CrossRef]
38. Ni, X.Q.; Kong, D.C.; Wen, Y.; Zhang, L.; Wu, W.H.; He, B.B.; Lu, L.; Zhu, D.Z. Anisotropy in mechanical properties and corrosion resistance of 316L stainless steel fabricated by selective laser melting. *Int. J. Min. Met. Mater.* **2019**, *26*, 319–328. [CrossRef]
39. Mantisi, B.; Sator, N.; Guillot, B. Structure and transport at grain boundaries in polycrystalline olivine an atomic-scale perspective. *Geochim. Cosmochim. Acta* **2017**, *219*, 160–176. [CrossRef]
40. Shi, F.; Gao, R.H.; Guan, X.J.; Liu, C.M.; Li, X.W. Application of grain boundary engineering to improve intergranular corrosion resistance in a Fe-Cr-Mn-Mo-N high-nitrogen and nickel-free austenitic stainless steel. *Acta Metall. Sin.* **2020**, *33*, 10. [CrossRef]